

Self Shielded Coil Homogeneity Analysis for the nEDM Experiment at TRIUMF

Roseanna Burrough

May 5, 2017

Abstract

The TRIUMF nEDM experiment aims to improve measurement of the neutron's electric dipole moment by an order of magnitude. The method to achieve this requires an extremely homogeneous magnetic field. Inhomogeneities of the applied $1\mu\text{T}$ magnetic holding field, B_0 , are expected to be one of the leading sources of systematic errors affecting the measurement. In order to achieve the desired B_0 field homogeneity of 0.1nT/m we are looking into employing a self shielded coil design, as this design does not interact magnetically with the surrounding experimental apparatus. Here two coils of different sizes with counter propagating currents work together to provide the B_0 field inside the measurement volume cell while canceling each other outside of the outer coil. One primary concern with employing self-shielded coils is to how accurate the building process has to be. To explore this we have been developing a self-shielded B_0 coil using the 3D finite element analysis program COMSOL to investigate how misplacements of the coil locations effect the overall homogeneity over the EDM cell.

1 Introduction

1.1 Why the nEDM experiment

The experiment was initially designed to test the symmetry of parity, which at the time was considered an inviolable symmetry.[14] The Electric Dipole Moment (EDM) of a system refers to the distribution of positive and negative charges within the system.

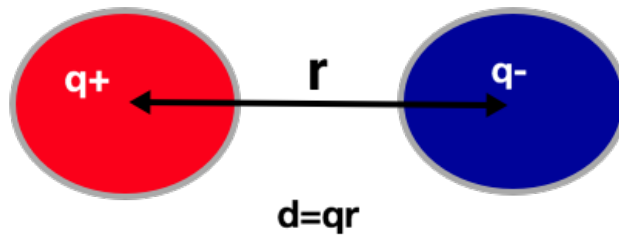


Figure 1: Diagram shows simplified dipole moment where, r is the distance between the charges, q is the magnitude of the charges and d it the dipole moment.

The EDM of a system with non degenerate (no two the same) ground states violates both time reversal and parity symmetries. Where the parity operator reflects a system through its origin meaning it changes left-handed coordinates into right-handed coordinates, the time-reversal symmetry is the symmetry of physical laws under a time reversal operation $t \rightarrow -t$ and charge conjugation turns a particle into its anti-particle $e^+ \rightarrow e^-$. In the 1950s Smith, Purcell and Ramsey developed and performed the first neutron electric dipole moment experiment. In the following decade charge-parity (CP) violation was linked to the time-reversal operator (T). This led to more investigation into symmetry relations which eventually led to Andrei Sarkarov's 1967 paper which outlined conditions required to explain the observed asymmetry of matter and anti-matter at the beginning of the universe. The Sarkarov

Criteria[10] are the following

1. Departure from thermal equilibrium
2. More CP violation than suggested in the standard model
3. Baryon number violation

Currently the standard model predicts an nEDM at approximately $10^{-31}\text{e}\cdot\text{cm}$. However, certain theoretical extensions beyond the standard model, such as super symmetry [6] predict an nEDM four orders of magnitude larger, at the $10^{-27}\text{-}10^{-28}\text{e}\cdot\text{cm}$ level. If a nEDM is discovered at these values, it would be heralded as a new system for CP violation and greatly enhance knowledge of physics beyond the standard model theories.

1.2 History of the nEDM Experiment

In the past 60 years there have been three different types of nEDM experiments. Figure 2 shows the nEDM upper limits plotted against the year of publication for these three methods. The different shapes of the markers represent the different measurement techniques described below.

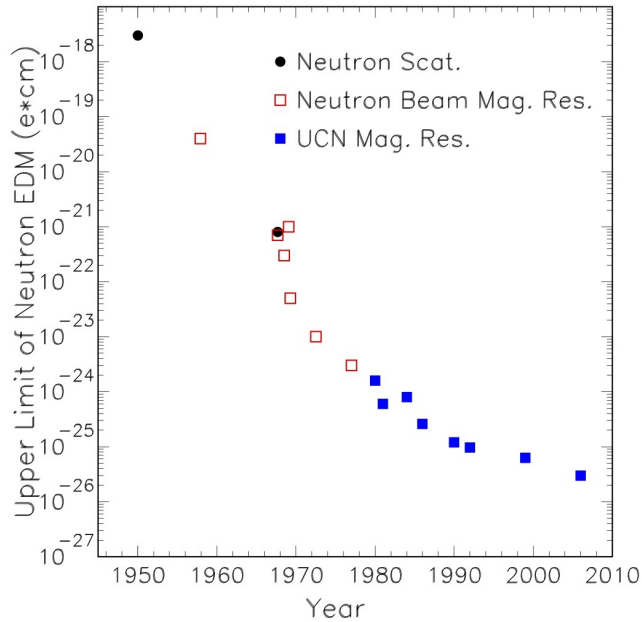


Figure 2: History of the nEDM experiment measured upper limits plotted against the year of the experiment. From this we see that the most precise measurements have been made in the last two decades using ultracold neutrons.

nEDM from Neutron Scattering (Upper limit $3 \times 10^{-18}e\cdot\text{cm}$ and $5 \times 10^{-22}e\cdot\text{cm}$)[3][4]

The first measurement of the nEDM was from neutron scattering experiments in 1950 by Purcell and Ramsey. They looked at the neutron-electron interaction deduced from the interference between neutron-nucleus and neutron-electron scattering. If the observed n-e interaction strength is given totally to the nEDM, then upper limit of can be measured as $d_n < 3 \times 10^{-18}e\cdot\text{cm}$. Another neutron scattering technique tested in 1967 by Shull and Nathan is Bragg reflection of thermal neutrons from a single crystal.[14] The scattering creates a magnetic field in the neutrons rest frame which interacts with the magnetic moment of the neutron resulting in Schwinger scattering. When the neutron has a non-zero EDM the coulomb field of the nucleus would lead to an additional potential $V(d_n) = -\vec{d}_n \cdot \vec{E}(r)$. The effect of nEDM

is maximized when the polarization lies on the scattering plane, since Schwinger scattering is maximized when the polarization is perpendicular to the scattering plane. This allows the isolation of the nEDM. With this method measuring Bragg reflection of polarized neutrons off a Cds crystal, an upper limit of $5 \times 10^{-22} \text{e}\cdot\text{cm}$ was set. The important limitation to this experiment is the difficulty in aligning the crystal to the polarization direction of the incident neutrons.

In Beam Magnetic Resonance (upper limit $3 \times 10^{-24} \text{e}\cdot\text{cm}$)[5]

Using the in beam magnetic resonance technique to measure the nEDM employs a magnetic resonance technique that was created by Alvarez and Bloch. Here the precession frequency of polarized cold neutrons (speed 152-1515m/s) is determined as they traverse a region with aligned/anti-aligned magnetic and electric fields via the Ramsey technique (described in section 1.3). This method's results are dominated by systematic errors caused by a misalignment of the magnetic and electric fields[12]. The results from this experiment gave an upper limit of $d_n < 3 \times 10^{-24} \text{e}\cdot\text{cm}$ which is two orders of magnitude smaller than the previously used methods.

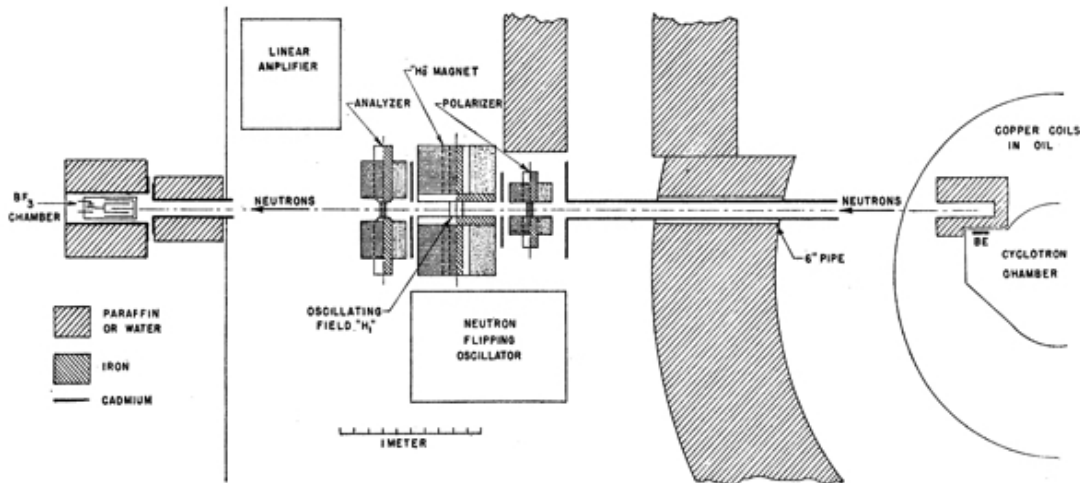


Figure 3: Apparatus for Alvarez and Bloch's[2] magnetic resonance technique.

Ultracold Neutron Resonance Measurement (upper limit $3 \times 10^{-26} \text{e}\cdot\text{cm}$)

Currently the best measurement of the nEDM took place in the ultra cold neutron facility at the Institut Laue-Langevin in Grenoble France in 1996. This measurement is very similar to the cold neutron beam measurements described above. However now the ultracold neutrons(UCN) are stored in a measurement cell with a much smaller volume, a homogeneous electric field and a homogeneous magnetic field applied to it. The Ramsey resonance technique described in Section 1.3 is then used to measure the precession frequency of the UCN. The results from this experiment are dominated by statistical errors, where the statistical variance in the nEDM data, shown in Equation 1, is inversely proportional to the the number of neutron sampled.

$$\sigma(d_n) = \frac{\hbar}{2\alpha ET\sqrt{N}} \quad (1)$$

Here α is the so-called visibility factor, and is related to the neutron polarization, $\hbar = \frac{h}{2\pi}$ where h is Planck's constant, E is the electric field, T is the precession time, and N is the total number of UCN in the sample. Obviously as long a precession time is desired. A precession time of 130 s was found to optimize the statistical precision. However this is in conflict with the lifetime of the neutrons in the measurement cell which is 100s. Using traditional methods of creating UCN, the quantity or number of neutrons (N) available for experimentation was relatively small leading to large statistical errors in the results.

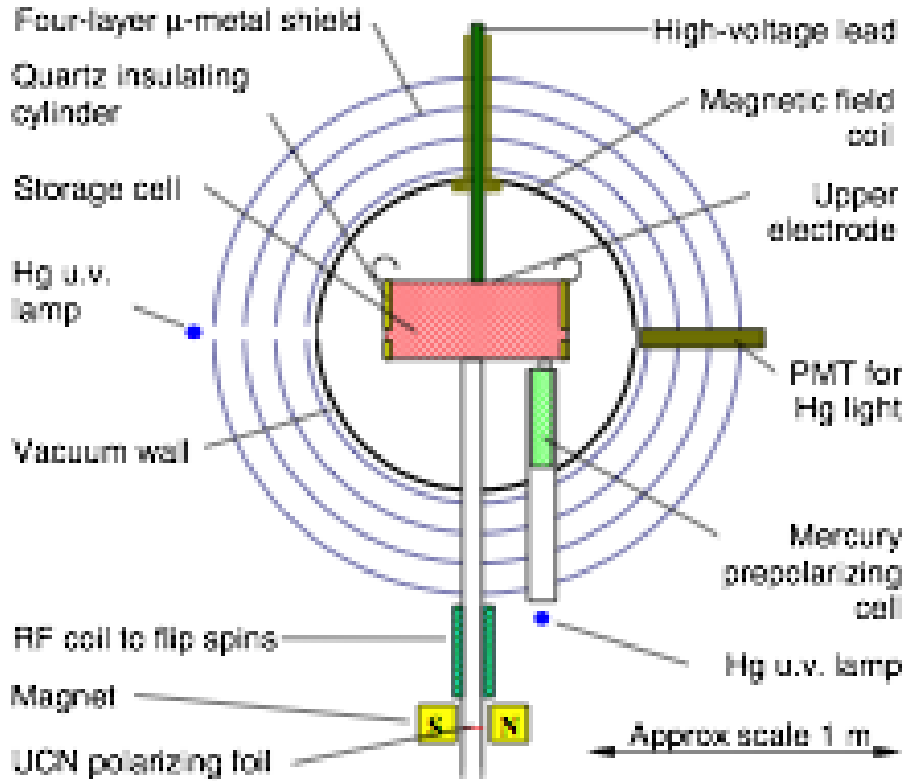


Figure 4: 2D drawing of the apparatus at ILL which uses UCN to measure nEDM[1]

1.3 Measurement Technique

All the nEDM magnetic resonance experiments described rely on the Ramsey resonance technique. Figure 5 depicts the Ramsey technique. The neutrons spin is polarized in the direction of a holding field, then an oscillating magnetic field which excites the neutron spins (B_1 field) within the cell and tips the spin of the neutron into the horizontal plane. This flips the neutrons's spins by $\frac{\pi}{2}$. The neutron is then left to precess freely for as long as possible (usually about 130s), then an equivalent B_1 is applied to flip the spin by another $\frac{\pi}{2}$.

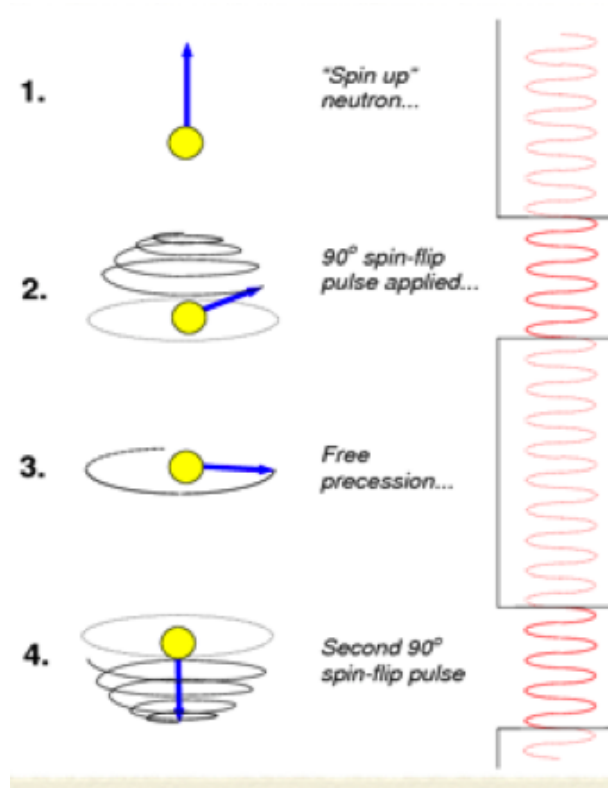


Figure 5: Visual representation of the flipping of the spins through the application of an oscillating magnetic field.

The following hamiltonian (neglecting gravity) can be used to describe a neutron in the presence of both a magnetic field and an electric field

$$H = -\mu_n \cdot \vec{B} - d_n \cdot \vec{E} \quad (2)$$

where μ_n is the neutrons magnetic moment, B is the magnetic field, E is the electric field and d_n is the nEDM. This can then be manipulated to extract the value of the nEDM by using the precession frequencies measured for the neutrons in the two opposite fields.

$$hf^{\uparrow\uparrow} = 2\mu_n B^{\uparrow\uparrow} + 2d_n E^{\uparrow\uparrow} \quad (3)$$

$$hf^{\uparrow\downarrow} = 2\mu_n B^{\uparrow\downarrow} - 2d_n E^{\uparrow\downarrow} \quad (4)$$

where h is Planck's constant and 2 up arrows signify an electric field in parallel with the magnetic field and one up and one down means anti-parallel to the magnetic field. Combining Equations 3 and 4 we get:

$$d_n = \frac{h(f^{\uparrow\uparrow} - f^{\uparrow\downarrow}) - 2\mu_n(B^{\uparrow\uparrow} - B^{\uparrow\downarrow})}{2(E^{\uparrow\uparrow} + E^{\uparrow\downarrow})} \quad (5)$$

Which can become Equation 6 if the magnetic fields completely cancel and the electric fields completely add, $E=E^{\uparrow\uparrow}=E^{\uparrow\downarrow}$.

$$d_n = \frac{h(f^{\uparrow\uparrow} - f^{\uparrow\downarrow})}{4E} \quad (6)$$

1.4 The Proposed nEDM experiment at TRIUMF

In order to counteract the statistical errors connected to the UCN measurement for the nEDM, a new method to produce high density of UCNs is being used. But a major concern for this experiment is the systematic error caused by the geometric phase effect (GPE). The GPE refers to the phase introduced to the spins of the polarized neutrons by inhomogeneities in the magnetic field. This GPE leads to a false nEDM given by Equation 7.

$$d_{nf} = -\frac{\hbar \langle v_n^2 \rangle}{4 c^2} \frac{1}{B_{0z}^2} \frac{\partial B_{0z}}{\partial z} \quad (7)$$

Where \hbar is the reduced Planck's constant, $\langle v_n^2 \rangle$ is the ensemble average velocity of the UCN, c is the speed of light and B_0 is the holding field. If the field gradient is suppressed down to $\partial B_{0z}/\partial z = 0.1 nTm^{-1}$, the false nEDM at $B_0=1\mu T$ and $\langle v_n^2 \rangle=2.4ms^{-1}$, is $d_{nf} = 2.1 \times 10^{-28} e \cdot cm$. This seems insignificant but as we aim for sensitivities on the order of $d_n=10^{-28}$ it becomes important. In order to minimize systematic errors from the above GPE effect we are aiming for a homogeneity

of $\partial B_0/\partial z < 0.1 \text{ nTm}^{-1}$. Figure 6 shows the relationship between field homogeneity and the magnitude of the false nEDM.

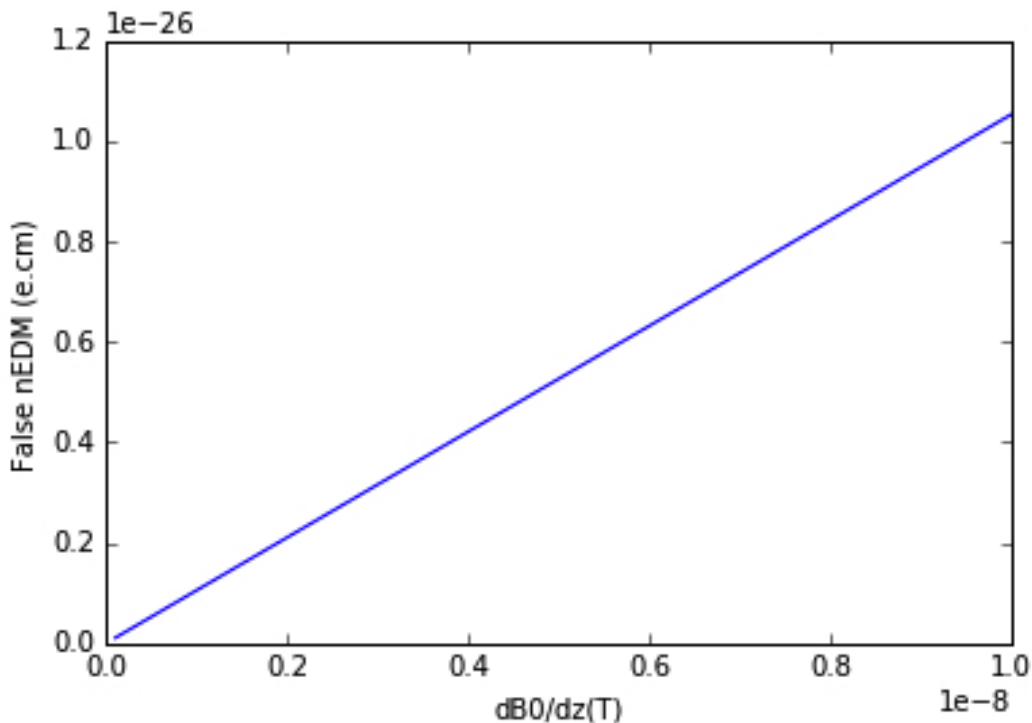


Figure 6: Graph represents the relationship between the value of the false nEDM and the inhomogeneities in the magnetic field $\partial B_0/\partial z$ assuming a $\langle v_n^2 \rangle = 2.4 \text{ m/s}$ associated with a quartz nEDM cell. Our experiment is aiming for a sensitivity of $10^{-27(28)}$, this requires a homogeneity in the holding field below 1 nT/m at least and much less than that for the 10^{-28} level

Past experiments have looked at using different materials for the nEDM cell. It is advantageous to use a material for the cell wall that will trap higher energy UCN because the distribution of neutrons created increases with approximately v^2 . Then a container made with a higher UCN velocity trapping material will increase the UCN statistics. However this increased velocity has a negative effect on the false nEDM, since as seen in Equation 7 that d_{nf} is proportional on $\langle v_n^2 \rangle$. In Figure 7, you can see a comparison of two materials, sapphire and quartz, and how important they are to field stability. Previously a field stability of 1 nT/m was desired and it can be

seen that there is a large difference between the false nEDM values in sapphire and in quartz. We are now aiming for 0.1nT/m, because at this homogeneity level the difference between the materials is within acceptable limits, less than $0.2 \times 10^{-28} e \cdot cm$. The ability to use the cell with a higher energy UCN could give new opportunities to reduce our statistical error through the increase of UCNs.

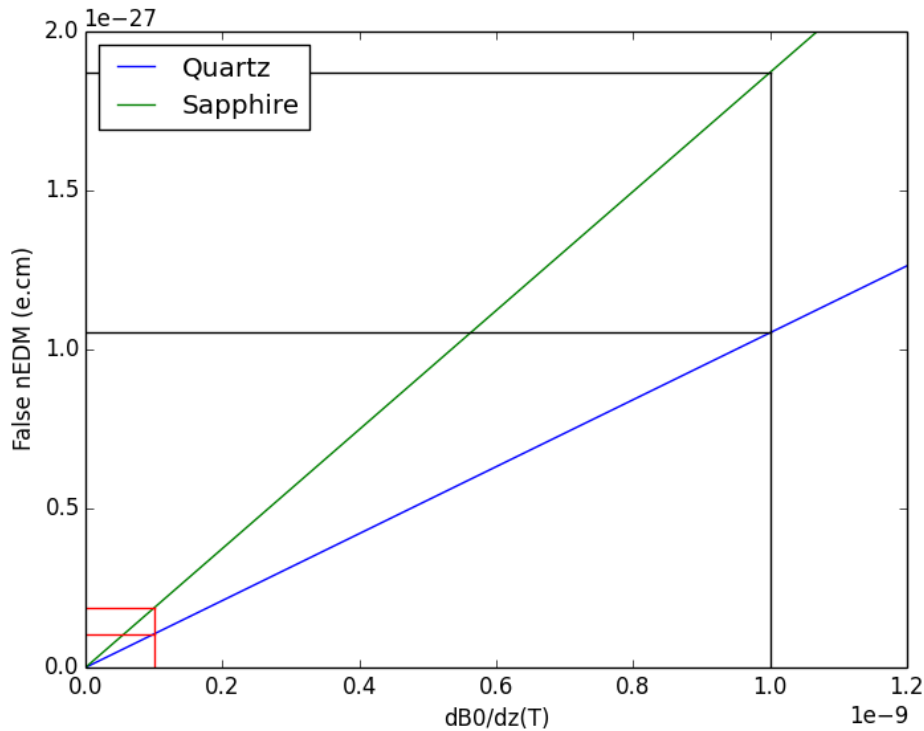


Figure 7: Graph represents the relationship between the value of the false nEDM and the inhomogeneities in the magnetic field $\partial B_0/\partial z$ along with a comparison between sapphire and quartz over 0.1nT/m to 1nT/m. We can see that at 0.1nT/m the sapphire cell falls within the $0.2 \times 10^{-28} e \cdot cm$ acceptable limit.

1.5 How to Achieve Homogeneity Specifications

To achieve the levels of homogeneity required, 0.1nT/m for the experiment we have looked at two different coil designs.

- **Shield Coupled Coil:** As shown in Figure 8a, a shield coupled coil consists of a coil creating the magnetic field surrounded by a magnetic shield that acts as a return yoke.
 - **Advantages:** This is the method that has been used multiple times in the past. It is well tested. The engineering tolerances for these designs are thought to be not as strict in comparison to the predicted build tolerances of the self shielded coil.
 - **Disadvantages:** The resulting holding field, B_0 , is time and environmentally dependent, so even minor fluctuations in the outside environment can have a big effect on the stability and homogeneity of the B_0 field over the measurement cell.
- **Self Shielded Coil:** As seen in Figure 8b, generally a self shielded coil is made up of two coils, one within the other. Here the outer coil has current running in the opposite direction to the inner coil. It creates a homogeneous magnetic field in the centre but the coils are spaced such that any field generated by the inner coil is cancelled outside of system.
 - **Advantages:** The magnetic field is isolated from its environment and is independent of any changes in the conditions surrounding the experiment.
 - **Disadvantages:** This method is untested with regards to our experiment, and there has been speculation as to whether the the manufacturing tolerances are too severe for accurate construction.

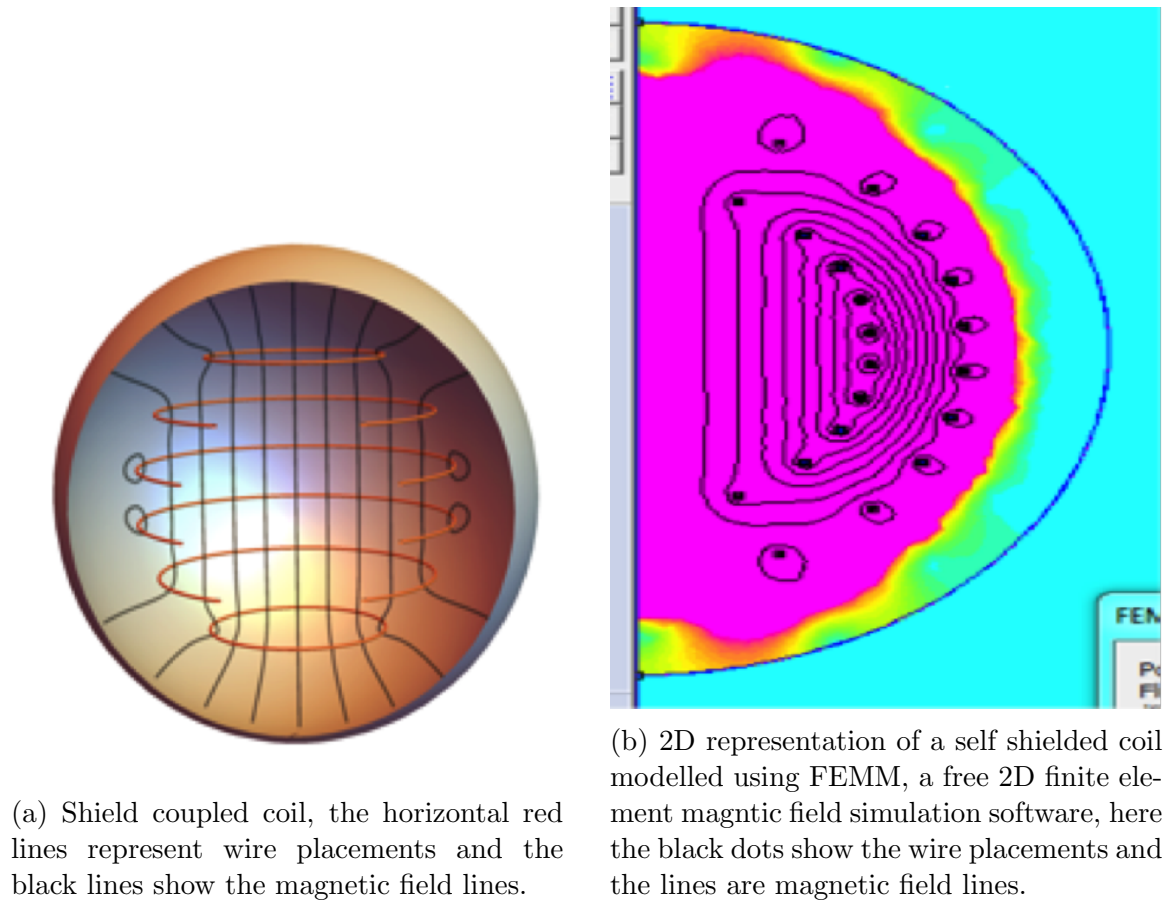


Figure 8

2 Theory

The purpose of this thesis is to develop a method for designing a self shielded B_0 coil for the nEDM experiment, and to develop a process to evaluate the fabrication tolerances required to meet a homogeneity specification of the magnet. We will use a finite element analysis software COMSOL to solve a complex set of differential equations with appropriately defined boundary conditions, derived below. It will tell us where current wires should be placed on the coil structure in order to achieve the desired B_0 field.

2.1 Derivation From Maxwells Equations

From Maxwells equations we have

$$\vec{\nabla} \cdot \vec{B} = 0 \quad (8)$$

$$\vec{\nabla} \times \vec{H} = \vec{J}_f \quad (9)$$

$$\vec{B} = \mu_0(\vec{H} + \vec{M}) \quad (10)$$

[9] Where \vec{B} is a magnetic field, \vec{H} is magnetic field strength, \vec{J}_f is current density, \vec{M} is Magnetization and μ_0 is permeativity of free space. If $\vec{J}_f = 0$ then $\vec{\nabla} \times \vec{H} = 0$. In free space $\vec{B} = \mu_0\vec{H}$ ($\vec{M} = 0$). This implies that from Equation 8 $\vec{\nabla} \cdot \vec{H} = 0$. $\vec{\nabla} \times \vec{H} = 0$ in free space, which means that \vec{H} it is a conservative field and as such the vector can be defined in terms of the scalar potential U:

$$\vec{H} = -\vec{\nabla}U \quad (11)$$

Then since $\vec{\nabla} \cdot \vec{H} = 0$ and the definition given in Equation 11 we can say $\vec{\nabla} \cdot (-\vec{\nabla}U) = 0$, and thus we see that U satisfies the Laplace equation

$$\nabla^2U = 0 \quad (12)$$

We seek to design a magnetic field generating coil, where in the space between the coils, Equation 12 applies. With this method of design the boundary conditions on the surface of the coil support structure are critically important: Here we have the important boundary conditions on a closed surface S:

$$\hat{n} \cdot [-\vec{\nabla}(\Delta U)] = 0 \quad (13)$$

$$\hat{n} \times [-\vec{\nabla}(\Delta U)] = \frac{4\pi}{c} \vec{K} \quad (14)$$

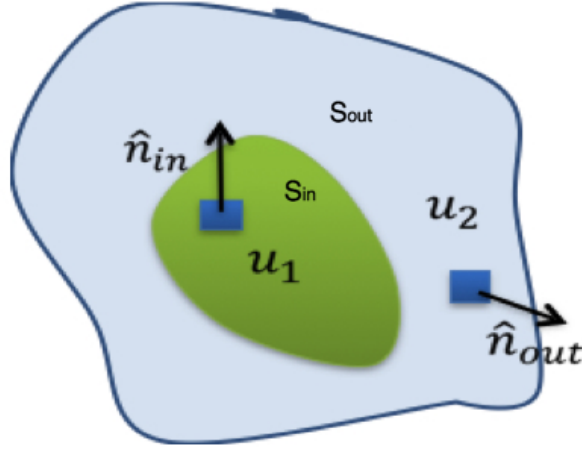


Figure 9: Example arbitrary surface S on which a surface current can run

where \vec{K} is the surface current density and $\Delta U = U_2 - U_1$ is evaluated on the relevant surface. Here U_1 is defined on the inner surface and U_2 on the outer surface as seen in Figure 9. From Equation 13 we see that flux is conserved over the outer surface meaning no field leaves the system and $-\vec{\nabla}(\Delta U)$ points along the surface S . Also due to the nature of gradients ($\vec{\nabla}$) we know that $-\vec{\nabla}(\Delta U)$ points along the steepest decrease in ΔU . From Equation 14 we see that the surface current must flow if the parallel component of \vec{H} along the surface is not conserved. \vec{K} also points along the surface but in the direction perpendicular to the steepest decrease in ΔU or more simply \vec{K} is parallel to contours of constant ΔU .

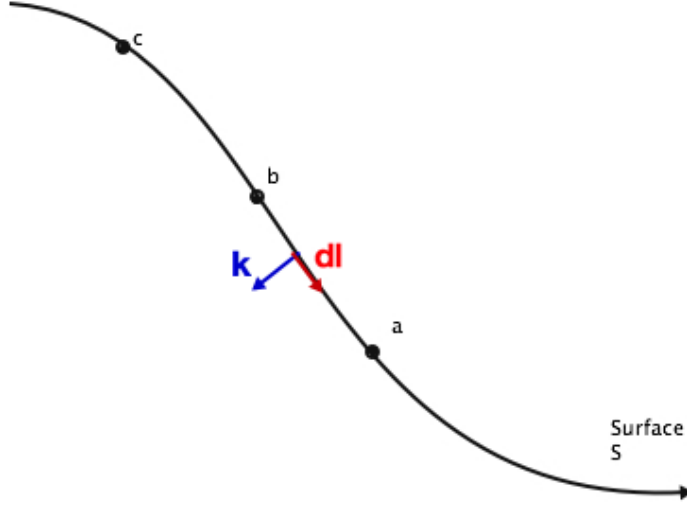


Figure 10: Side view cross section diagram, of an arbitrary surface S with surface current \vec{K} running along the it.

Next we will see how we can connect constant values of ΔU to a specific surface current. From the surface in Figure 10 consider integrating from a to b along $-\vec{\nabla}(\Delta U)$.

$$\int_a^b [-\vec{\nabla}(\Delta U)] \cdot d\vec{l} = -(\Delta U_b - \Delta U_a) \quad (15)$$

Where $d\vec{l}$ is parallel to $-\vec{\nabla}(\Delta U)$. This takes you from one contour of constant ΔU containing point a to another containing point b. Then using the relationship described in Equations 13 and 14 we can say.[15]

$$\begin{aligned} (\hat{n} \times [-\vec{\nabla}(\Delta U)]) \times d\vec{l} &= \frac{4\pi}{c} \vec{K} \times d\vec{l} \quad (16) \\ [(\hat{n} \times [-\vec{\nabla}(\Delta U)]) \times d\vec{l}] \cdot \hat{n} &= \frac{4\pi}{c} (\vec{K} \times d\vec{l}) \cdot \hat{n} \\ [-\vec{\nabla}(\Delta U)] \cdot d\vec{l} &= -\frac{4\pi}{c} (\vec{K} \times d\vec{l}) \cdot \hat{n} \end{aligned}$$

Combine this result with result from Equation 15 gives

$$(\Delta U_b - \Delta U_a) = -\frac{4\pi}{c} \int_a^b (\vec{K} \times d\vec{l}) \cdot \hat{n} \quad (17)$$

So the difference in ΔU 's, $\Delta(\Delta U)$ is equivalent to the surface current between a and b. Since \vec{K} is perpendicular to $d\vec{l}$ all along the path we can make the statement:[15]

$$\int_a^b (\vec{K} \times d\vec{l}) \cdot \hat{n} = -I \quad (18)$$

Where I is the current flowing between the contours containing a and b. If you then continue to the point c and if the contours are equally spaced ($\Delta U_c - \Delta U_b = \Delta U_b - \Delta U_a$) then the same current should flow between contours b and c. If you then approximate the surface current with discrete wires containing the current I then the windings of this wire should be equally spaced in contours of constant ΔU .

2.2 A Method to Design a Self Shielded Coil

The goal of this design is to produce a uniform magnetic field inside the green volume, U_1 with surface S_{in} , of figure 6 and no field outside the blue volume, U_2 with the surface S_{out} . This is achieved in the following 3 steps:

1. Using the derivations in the previous section we require that the boundary of S_{in} follows

$$-\vec{\nabla} U_1 \cdot \hat{n}_{in} = H_0 \hat{k} \cdot \hat{n}_0 = H_n n_{inz} \quad (19)$$

Then solve Laplace's equation internal to S_{in}

- Specify the boundary conditions on U_2

$$-\vec{\nabla}U_2 \cdot -\hat{n}_{in} = H_0\hat{k} \cdot \hat{n}_{in} \quad (20)$$

$$-\vec{U}_2 \cdot \hat{n}_{out} = 0 \quad (21)$$

Where Equation 20 covers flux conservation and Equation 21 deals with flux conservation in the case of a superconducting boundary condition making the field parallel to S_{out} everywhere and containing the flux.

- Determine equally spaced contours of $\Delta U_{inner} = U_2 - U_1$ on the inner surface and of $\Delta U_{outer} = U_2$ on the outer surface. These contours give the appropriate winding patterns for the wires.

3 Coil Design

As part of our coil design process we are using the finite element analysis (FEA) program COMSOL. A FEA (also known as the Finite Element Method) is a numerical technique that calculates the approximate solutions to partial differential equations under specific boundary conditions. It breaks the complex problems into smaller much simpler parts called finite elements. The simple equations that describe the finite element are then assembled into a large system of equations that model the entire system. FEA then uses variational methods from the calculus of variations to approximate a solution.

3.1 How to use COMSOL to Design a Closed Coil Surface

Comsol uses the method described above to find appropriate wire placements on a surface, coil form, that will make up the self shielded coil. The following is a general

example of a double cylinder self shielded coil.

- The first step is to define the 3D structures that the coil will be based on, in this case 2 cylinders shown below.

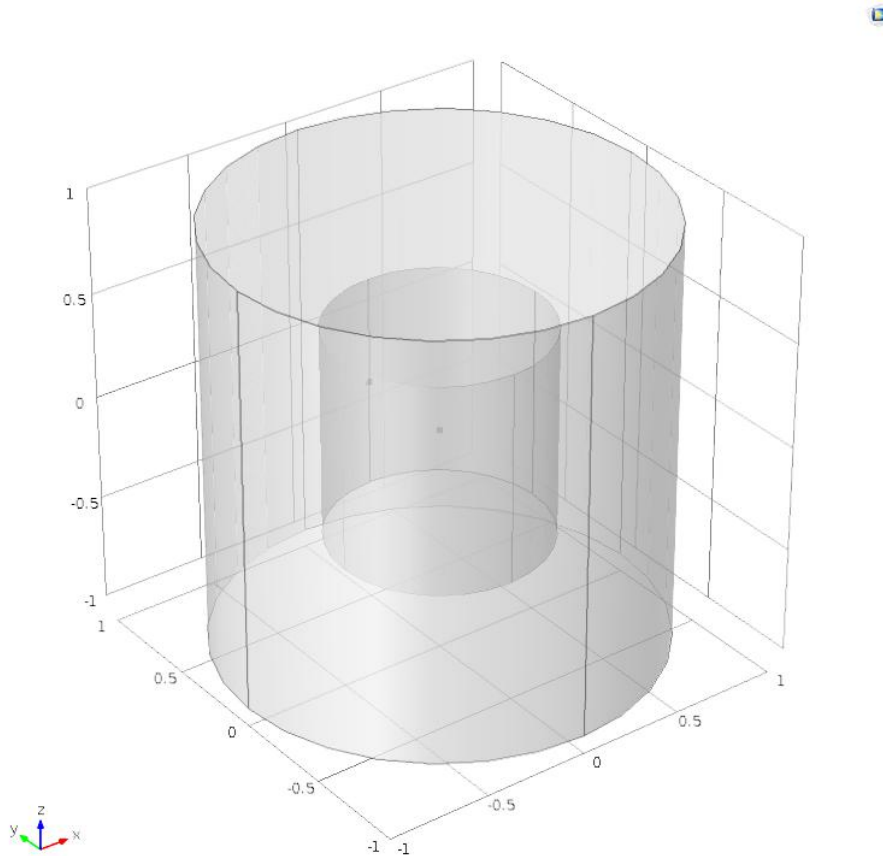


Figure 11: Diagram that shows double cylinders created in COMSOL

- Once the surface is created its time to define the boundaries. One starts by setting the boundaries/surfaces that will experience non-zero flux. These can be selected through the interface.
- At this point we introduce the Laplace equation to each of the surface components where Equations 19, 20 and 21 apply to the surfaces seen in Figure 12.

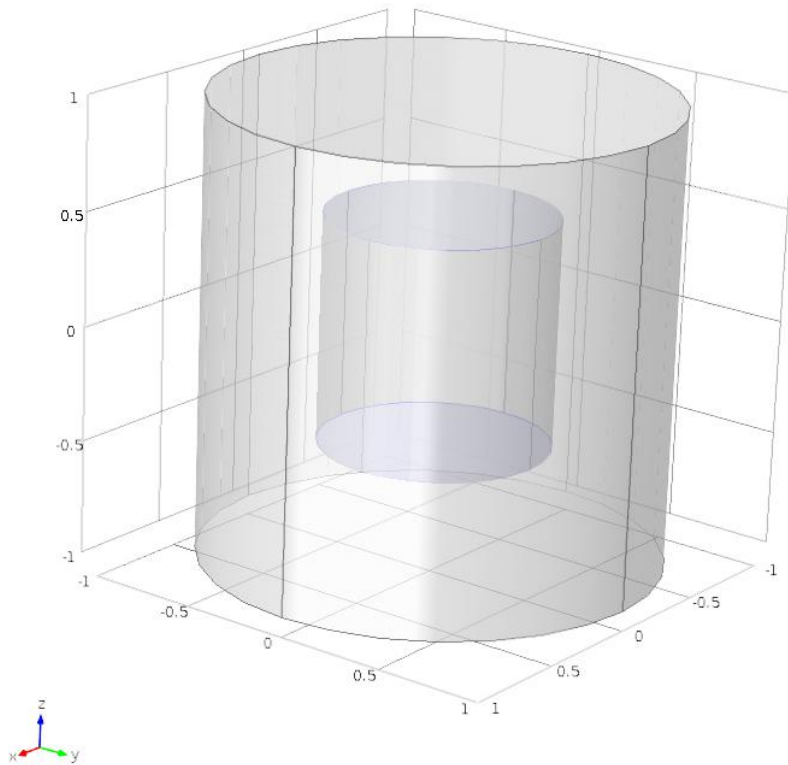


Figure 12: Diagram that shows the surfaces that have nonzero flux

- Then you use the solve command to solve the Laplace equation, Equation 12, with the boundary conditions described above.
- The results for this process can be seen below for a double cylinder design. Figure 13a shows the so called IsoLevels which are equivalent to the surfaces of constant $\Delta\Delta U$ and Figure 13b shows the optimal divisions of surface current

We then export the placements of the isolevels that have been determined by COMSOL into a data file consisting of a list of coordinate points that describe the wire placements. These placements can then be used to calculate the magnetic field and the homogeneity level of the coil.

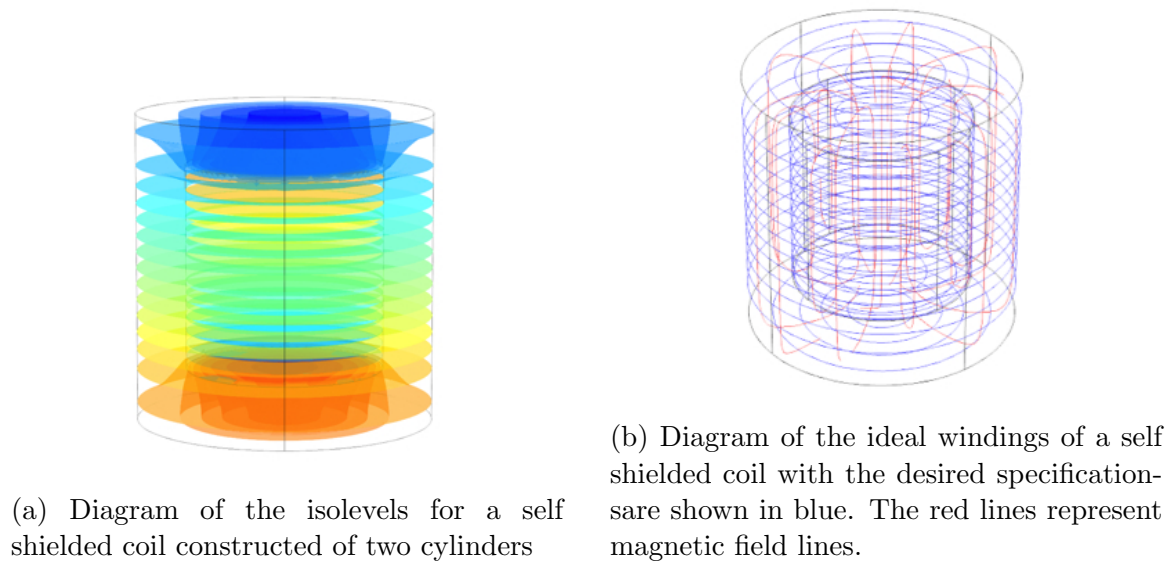


Figure 13

4 Field Analysis

For our experiment we designed a self shielded coil made from two boxes in COMSOL. Figure 14 show the Iso Levels for the main coil of our design and the ideal windings.

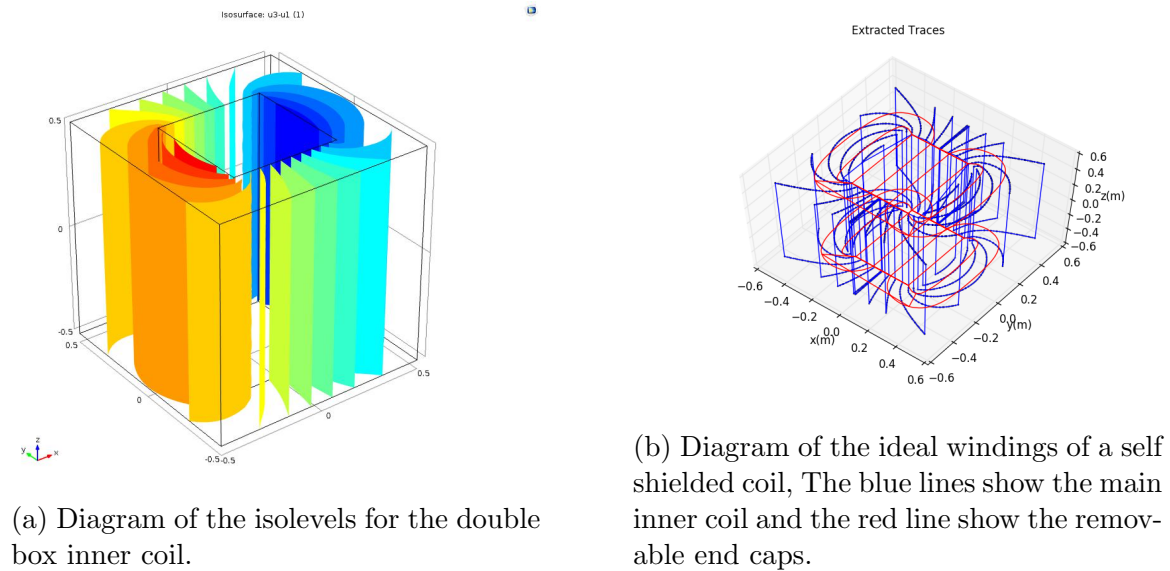


Figure 14

4.1 Sorting points

Unfortunately, COMSOL exports the isolevel points in an unhelpful order. Figure 15, shows the end face of the design shown in Figure 14a where the positions of the isolevels were exported and plotted with connecting lines. While the general shape can be seen, some of the points do not line up consecutively so they do not make the required continuous wire.

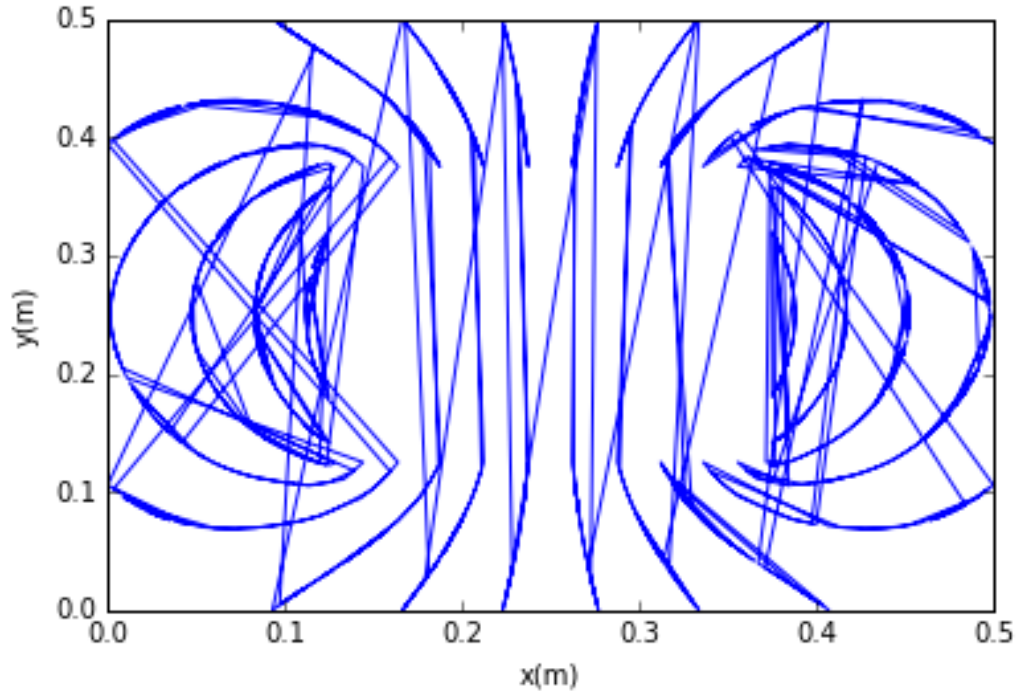


Figure 15: Shows the results of plotting the raw output from COMSOL

The first step in analyzing the models is to sort the points into a more convenient order and format. This is achieved using a program written in python. In order to simplify the sorting process we only take a quarter of the boxes face created in COMSOL. Figure 16 shows the first quarter after it has been put through the sorting program. The next step was to extend the model in the z-direction to recreate the 3D model. Figure 17 shows this extension so we now had a fully sorted quarter of the box.

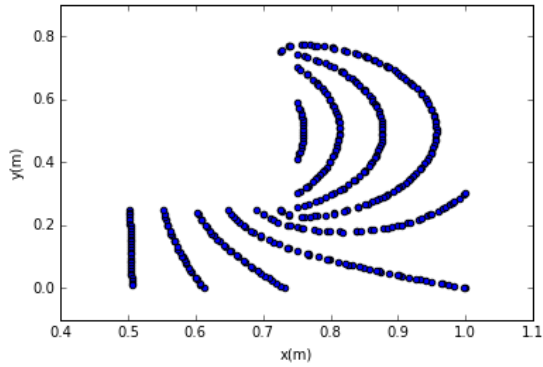


Figure 16: Placements for coils in the first quarter of the coil

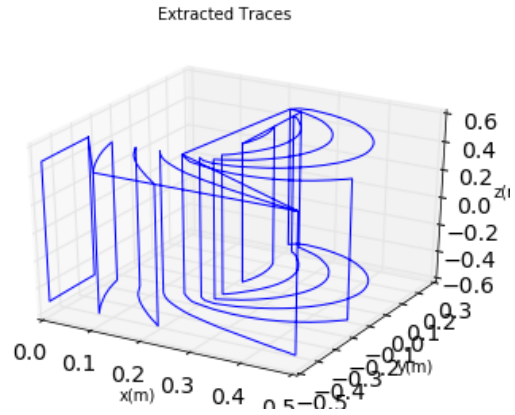


Figure 17: Extension of end face in the z direction

Then we use symmetry to build the entire model using another python script. First we copy the model and introduce a negative to the y-components, then reverse the order of the points and concatenate them onto the original quarter. Figure 18 shows the now half model. Repeating this process but introducing the negative into the x-components we flip over the y-axis in order to gain the full model seen in Figure 19.

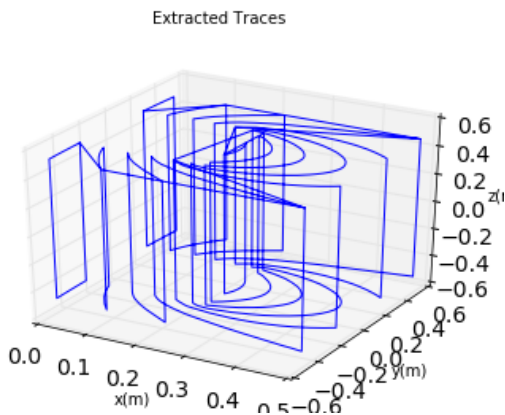


Figure 18: half point in build process

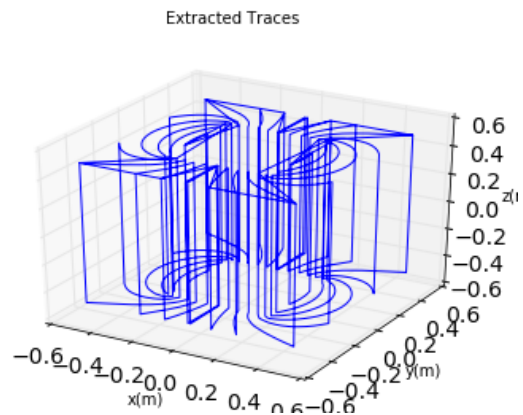


Figure 19: Full inner coil

The coil so far is not completely self shielded. So called "end caps", wires on the faces of the coil structure, need to be in place. The above process is then partial repeated with these caps as seen in Figure 20. The end caps are in general simple

enough that they can be sorted as a whole. End caps have the advantage that they are removable so that they can be taken on and off to allow inserted of the nEDM cell.

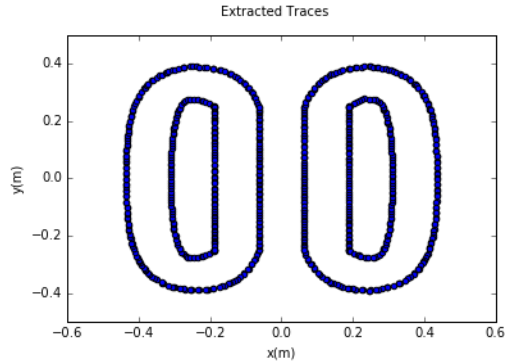


Figure 20: Outer removable endcap

4.2 Biot Savart

Now that we have a coil whose wire position are correctly sorted we can calculate the magnetic field it creates. We use a Biot Savart calculation to model the magnetic field because it is very versatile and independent of shape. It assumes that the coil can be defined as a series of straight line segments. The Equation 22 is used to calculate the field for each segment. Then due to the cumulative nature of magnetic field, by summing over all of the segments we can gain the magnetic field for the entire coil.[8]

$$B = \frac{\mu_0 I}{4\pi} \hat{e} \times R_i \frac{2L(R_i + R_f)}{R_i R_f} \frac{1}{(r_i + R_f)^2 - L^2} \quad (22)$$

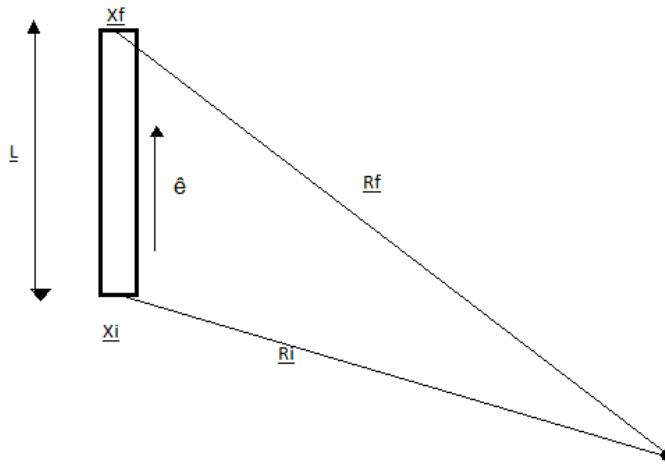


Figure 21: Diagram defining variables for Equation 22 for Biot Savart

As seen in Figure 22, using this calculation technique we find the magnetic field of the double cosine theta box can be found. This figure shows the z component of the magnetic field along the z-axis over a region of interest of 50cm in the centre of the coil.

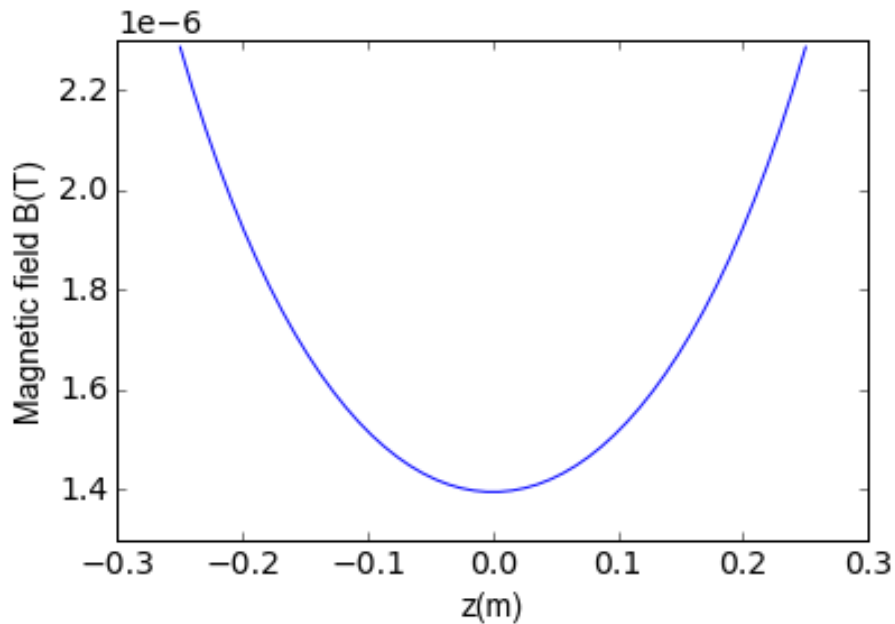


Figure 22: Graph shows the magnetic field along the z-axis within a region of interest $-0.25\text{m} < z < 0.25\text{m}$. With current $I_1=2\text{A}$ on the inner Coils and $I_2=1.2\text{A}$ on the end caps

Once the magnetic field is calculated it is time to measure the homogeneity. This is achieved by looking at the gradient of the magnetic field ∇B_z . We can look at just the z component of the magnetic field since the x and y are small enough to be ignored. Figure 23 shows the gradient of the B_{0z} field along the z-axis. The gradient is important as a way to quantify the inhomogeneity of the magnetic field.

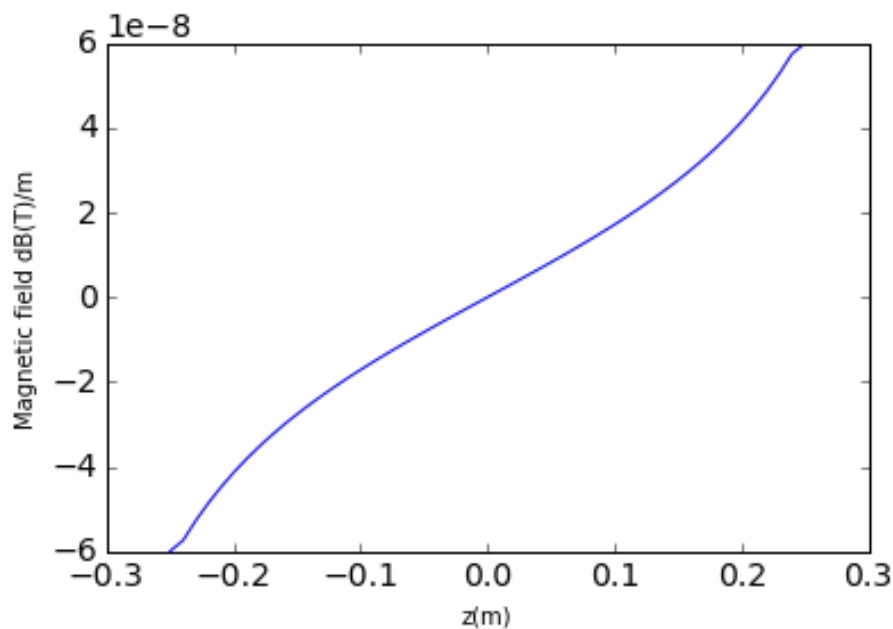


Figure 23: Graph shows the change in the magnetic field along the z-axis within a region of interest $-0.25\text{m} < z < 0.25\text{m}$. With current $I_1=2\text{V}$ on the inner Coils and $I_2=1.2\text{V}$ on the end caps

5 Wire Displacement Investigation

After creating the tools to analyze the magnetic field created by a specific coil we then start looking at how moving wires in the coil effects the magnetic field. Figures 25-27 show the magnetic field and gradient of the magnetic field of the coil along the z-axis within our 50cm region of interest, with a shifted current loop.

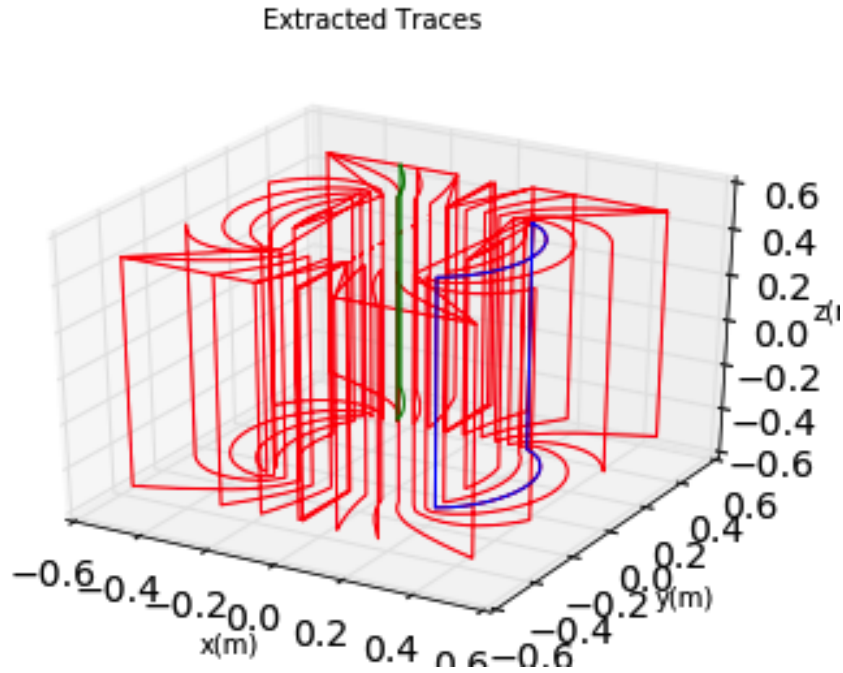
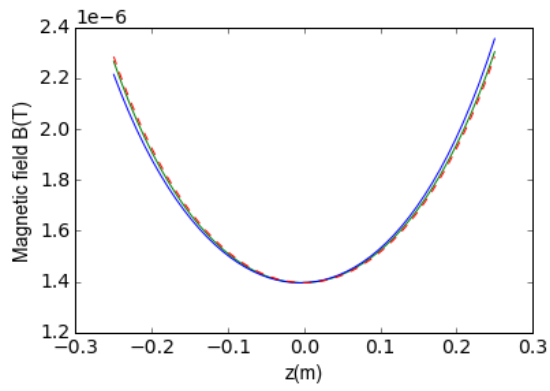


Figure 24: Representation of the current loops being shifted on the inner coil in the following studies. The end caps are not show to simplify the diagram, but they are include in the calculation.

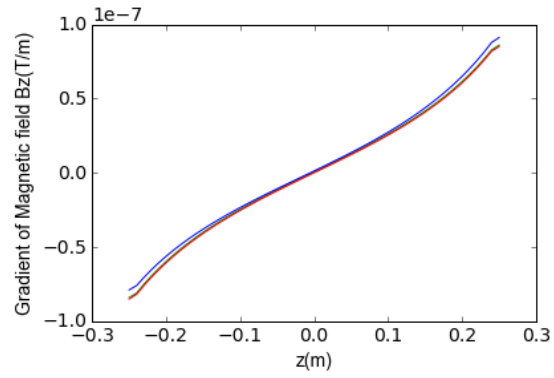
For the figures in the following four sections the red dashed lines represent the magnetic field from the original coil, the blue and green represent the magnetic field after shifts in the corresponding current loops from Figure 24.

5.1 Coil Shift in the x-Direction

Figure 25 represents the field the current loop has been shifted by 5cm in the -x direction.



(a) Magnetic field along z-axis after a x-direction shift

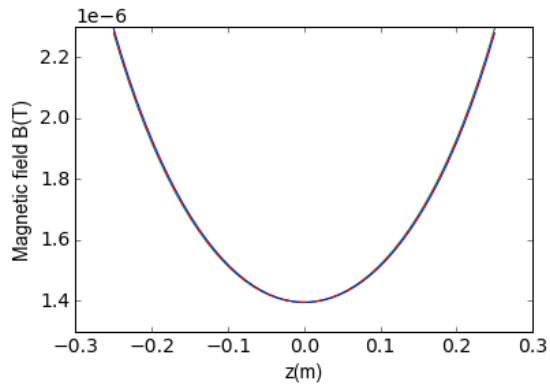


(b) Gradient of the magnetic field shown in part (a)

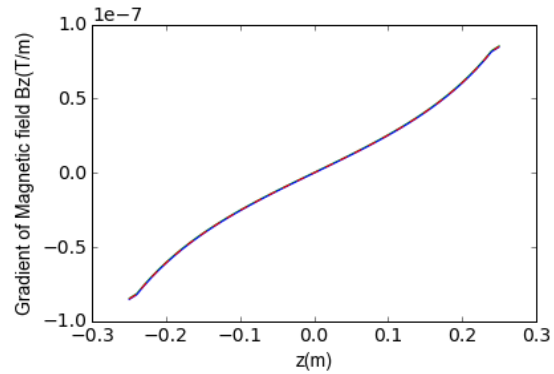
Figure 25

5.2 Coil Shift in the y-Direction

Figure 26 represents the field when the current loop has been shifted by 5cm in the -y direction



(a) Magnetic field along z-axis after a y-direction shift

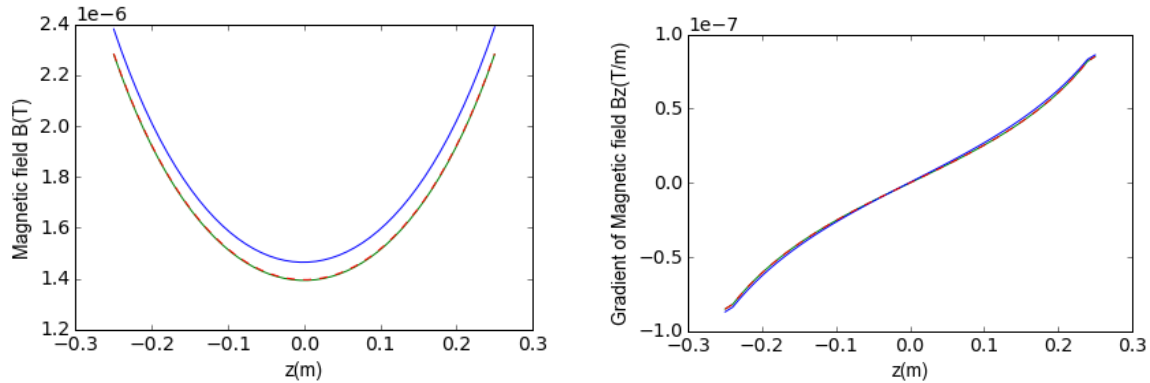


(b) Gradient of the magnetic field shown in part (a)

Figure 26

5.3 Coil Shift in the z-Direction

Figure 27 represents the field when the current loop has been shifted by 5cm in the -z direction



(a) Magnetic field along z-axis after a z-direction shift

(b) Gradient of the magnetic field shown in part (a)

Figure 27

From sections 5.1 to 5.3 we see that shifts in the x and z direction have more effect on the gradient curve than the y direction shift. It is also obvious that moving blue loop has a greater effect on both gradient and magnitude of the magnetic field; This makes sense as the blue coil is longer and therefore contributes more to the field at the centre of the than the green coil.

5.4 Coil Removal

Figure 28 show the resulting magnetic field after removing a loop from the coil. This removal is achieved by shifting the current loop to a relatively large distance away until it is no longer interacting with the rest of the coil.

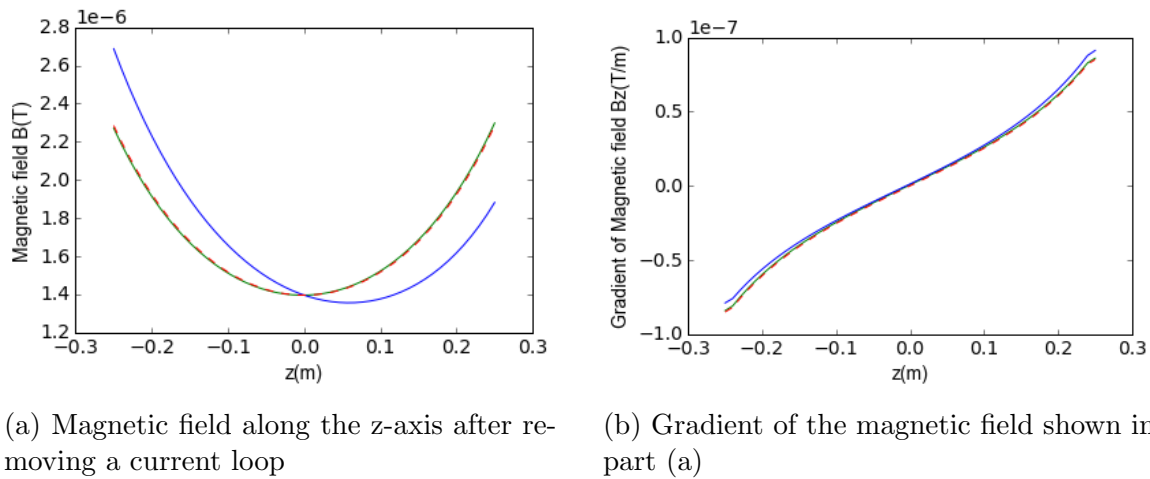


Figure 28

This shows that there is a significant difference in the impact of which current loop is being displaced. It also shows how easily asymmetry can be introduced into the magnetic field. The differences in the gradients for all the changes are relatively small compared to the total magnitude of the inhomogeneity. The magnetic field is currently dominated by a quadratic term which must be minimized in order to get closer to our specifications. In the future we will work on optimizing the coil design to reduce the inhomogeneities down to $dB_{0z}/dz < 10^{-9} T/m$ at which time those small changes seen in the figures will become a lot more significant.

6 Conclusion

In order to motivate an explanation for the matter/anti-matter asymmetry at the beginning of the universe scientists have been trying to accurately measure the neutron electric dipole moment. To meet the magnetic requirements to achieve this we used a finite element analysis program to design a double box self shielded coil. Then we created the tools to analyze the field, and gradient of the fields' tolerances to variances in current placement. It is seen that at the current level of homogeneity there is a relatively high tolerance to wire movement. However this is because the magnetic field is currently very inhomogeneous. In the future the design will be optimized to improve homogeneity and reduce the gradient of the magnetic field. Then with the tools displayed above more studies and comparisons will be made in order to define the necessary build tolerance for a successful manufacturing of the coil design with the desired magnetic field requirements.

References

- [1] C.A.Baker *et al.*, *An Improved experimental limit on the electric dipole moment of the neutron* Phys. Rev. Lett. **97**, 131801 (2006)
doi:10.1103/PhysRevLett.97.131801 [hep-ex/0602020]
- [2] Alvarez, Luis W. and Bloch, F.A *Quantitative Determination of the Neutron Moment in Absolute Nuclear Magnets*, Phys. Rev., 57, 2, 111–122, 0, 1940, Jan, American Physical Society, 10.1103/PhysRev.57.111, <https://link.aps.org/doi/10.1103/PhysRev.57.111>
- [3] E. M. Purcell and N. F. Ramsey, Phys. Rev. 78, 807 (1950), DOI: 10.1103/PhysRev.78.807
- [4] C. G. Shull and R. Nathans, Phys. Rev. Lett. 19, 384 (1967), DOI: 10.1103/PhysRevLett.19.384
- [5] W. B. Dress, Phys. Rev. D 15, 9 (1977), DOI: 10.1103/PhysRevD.15.9
Read More: <http://www.worldscientific.com/doi/ref/10.1142/S0217732308027771>
- [6] Filippone, B. nEDM Collaboration. *Search for a Neutron Electric Dipole Moment at the SNS*
- [7] , J.Byrne. *Nuclei and Matter: An Exploration of the Physics of Slow* Dover Publications, 2011.
- [8] Hanson, J. D. and Hirshman, S. P. *Compact expressions for the Biot-Savart fields of a filamentary segment* Phys.Rev.A9, Oct 2002, Physics of Plasmas, <http://adsabs.harvard.edu/abs/2002PhPl...9.4410H>
- [9] Griffiths, David J, *Introduction to electrodynamics; 4th ed.*, Pearson, Boston, MA, 2013

- [10] Konaka *Proposal*, 2011
- [11] T.Momose *Project Summary Neutron Electric Dipole Moment Experiment and Facility* The University of British Columbia, 2014
- [12] Pendlebury, J. M. and Heil, W. and Sobolev, Yu. and Harris, P. G. and Richardson, J. D. and Baskin, R. J. and Doyle, D. D. and Geltenbort, P. and Green, K. and van der Grinten, M. G. D. and Iaydjiev, P. S. and Ivanov, S. N. and May, D. J. R. and Smith, K. F., *Geometric-phase-induced false electric dipole moment signals for particles in traps*, Phys. Rev. A, 70, 3, sept 2004, American Physical Society, <http://link.aps.org/doi/10.1103/PhysRevA.70.032102>
- [13] J. M. Pendlebury *et al.*, *Revised experimental upper limit on the electric dipole moment of the neutron*, Phys. Rev. D **92**, no. 9, 092003 (2015) doi:10.1103/PhysRevD.92.092003 [arXiv:1509.04411 [hep-ex]].
- [14] Jen-Chieh Peng, *Neutron Dipole Moment Experiments* Modern Physics Letters A (c) World Science Publishing Company. April 8, 2008
- [15] Haus, Hermann A. and Melcher, James R. , *Electromagnetic fields and energy* , 013249020 0132492776 , Prentice Hall Englewood Cliffs, N.J , xxiii, 742 p Chapter 8 : , 1989 , Book , English , Electromagnetic fields.; Electrostatics.; Magnetostatics.; Electrical engineering. , 1989 - , <http://nla.gov.au/nla.cat-vn1680975>